Faraday Discussions

Accepted Manuscript

This manuscript will be presented and discussed at a forthcoming Faraday Discussion meeting. All delegates can contribute to the discussion which will be included in the final volume.

Register now to attend! Full details of all upcoming meetings: http://rsc.li/fd-upcoming-meetings

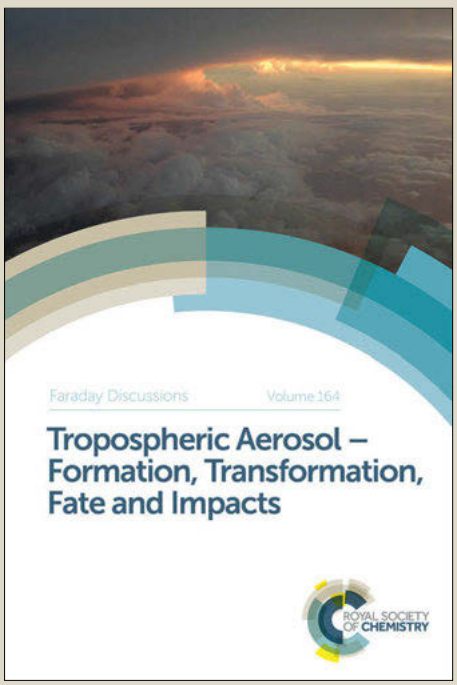

This is an *Accepted Manuscript*, which has been through the Royal Society of Chemistry peer review process and has been accepted for publication.

Accepted Manuscripts are published online shortly after acceptance, before technical editing, formatting and proof reading. Using this free service, authors can make their results available to the community, in citable form, before we publish the edited article. We will replace this *Accepted Manuscript* with the edited and formatted *Advance Article* as soon as it is available.

You can find more information about *Accepted Manuscripts* in the Information for Authors.

Please note that technical editing may introduce minor changes to the text and/or graphics, which may alter content. The journal's standard Terms & Conditions and the Ethical guidelines still apply. In no event shall the Royal Society of Chemistry be held responsible for any errors or omissions in this *Accepted Manuscript* or any consequences arising from the use of any information it contains.

ROYAL SOCIETY OF CHEMISTRY

www.rsc.org/faraday_d

CREATED USING THE RSC REPORT TEMPLATE (VER. 3.1) - SEE WWW.RSC.ORG/ELECTRONICFILES FOR DETAILS
Faraday Discussions
REVIEW www.rsc.org/xxxxxx | XXXXXXXX

Nanodiamond surface redox chemistry: influence of physicochemical properties on catalytic processes

Thomas S. Varley, [a]* Meetal Hirani, [a] George Harrison [a] and Katherine B. Holt. [a]*

DOI: 10.1039/b000000x

Modification of an electrode with an immobilised layer of nanodiamond is found to significantly enhance the recorded currents for reversible oxidation of ferrocene methanol (FcMeOH). Current enhancement is related to nanodiamond diameter, with enhancement increasing in the order 1000 nm < 250 nm < 100 nm < 10 nm < 5 nm. We attribute the current enhancement to two catalytic processes: i) electron transfer between the solution redox species and redox-active groups on the nanodiamond surface; ii) electron transfer mediated by $FcMeOH^+$ adsorbed onto the nanodiamond surface. The first process is pH dependent as it depends on nanodiamond surface functionalities for which electron transfer is coupled to proton transfer. The adsorption-mediated process is observed most readily at slow scan rates and is due to self-exchange between adsorbed $FcMeOH^+$ and FcMeOH in solution. $FcMeOH^+$ has a strong electrostatic affinity for the nanodiamond surface, as confirmed by *in situ* infrared (IR) experiments.

1. Introduction

In recent years electrochemical experiments have been undertaken using electrodes composed of, or modified with, undoped nanodiamond materials [1]. Given that bulk diamond is intrinsically insulating, with a band gap of 5.47 eV, it may seem unlikely that undoped diamond can perform as an electrode material. However, unsaturated bonding at the diamond surface and the presence of oxygen functionalities can give rise to surprisingly rich redox chemistry [2,3]. For diamond nanomaterials the large surface atom to bulk atom ratio allows surface properties to dominate, hence nanodiamond is able to participate in electrochemical processes despite its insulating nature. Different types of nanodiamond with varying surface termination have been investigated for electrochemical activity [1-5]. Most commonly used are detonation nanodiamond powders that have been used to construct cavity electrodes [5-7], sintered into pellet electrodes [8] or drop-coated from solution onto electrodes [2,3,9]. Detonation nanodiamond is synthesised by detonation of carbon-based explosives in the absence of oxygen, resulting in a carbonaceous soot from which the nanodiamond powder can be extracted and purified [10]. The resulting powder is composed of relatively monodisperse diamond nanoparticles, with average diameter of 5 to 10 nm, as shown in the TEM image in Figure 1 a. Detonation nanodiamond exhibits an array of surface carbon-oxygen functionalities (including ketone, esters, alcohols and acids) that have been characterised using FTIR [11,12] and XPS [13,14].

Electrodes modified with an immobilised surface layer of detonation nanodiamond show enhanced, catalytic electrochemical response towards various analytes such as nitrite [7], oxygen [15] and haemoglobin [16], as well as common redox probes like $Ru(NH_3)_6^{3+/2+}$ and $Fe(CN)_6^{3-/4-}$ [2,3,9].

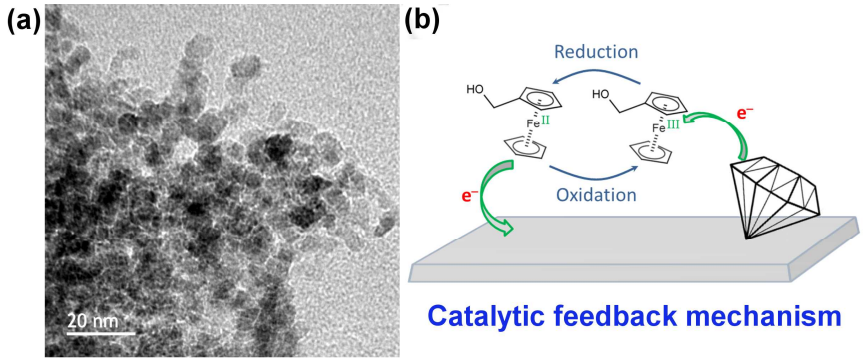

Fig. 1 – (a) TEM micrograph of 10 nm nanodiamond. (b) Illustration of the nanodiamond feedback mechanism. The green arrows depict the direction of electron transfer.

It is proposed that surface functionalities, defect sites and unsaturated bonding give rise to surface electronic states with energies within the band gap of undoped diamond [3]. It has been demonstrated that these surface states can act as both electron donors and acceptors and can support catalytic redox processes in the presence specific redox-active molecules via a feedback mechanism [1-3,9]. This mechanism is illustrated schematically in Figure 1 b. Briefly, a species such as FcMeOH can undergo oxidation at an electrode to produce $FcMeOH^+$. In the presence of nanodiamond, the $FcMeOH^+$ may then be reduced by redox active functionalities on the nanodiamond surface, resulting in regeneration of FcMeOH. This continual regeneration of FcMeOH in the electrode diffusion layer results in an enhanced catalytic current. In situ IR studies of 5 nm diameter nanodiamond in the presence of redox probes have implicated surface quinone- and hydroquinone- like moieties in this redox mediation [11]. Catalytic current enhancements at nanodiamond-modified electrodes, via the mechanism shown in Figure 1 b, have previously been reported for charged species such as $Ru(NH_3)_6^{3+/2+}$ and $Fe(CN)_6^{3-/4-}$ [3,9]. At nanodiamond-modified electrodes peak currents for these species increase 2-4 fold over diffusion-controlled currents at the unmodified electrode [1-3,9]. However, as the charge on the nanodiamond surface changes with protonation state of surface functionalities electrostatic interactions between surface and redox probe must be taken into account when carrying out analysis.

In this paper we focus on nanodiamond materials of different size and morphology and their interaction with the outer-sphere and uncharged redox probe FcMeOH. We find that electrodes modified with nanodiamond exhibit significantly enhanced catalytic currents for the reversible oxidation of this neutral species compared to charged redox species. We investigate the electrochemical response when changing the diameter of the nanodiamond particles used and the pH and ionic strength of the electrolyte solution. Analysing the effect of these physicochemical parameters, alongside factors such as redox species concentration and voltammetric scan rate, provides further insight into the mechanisms of current enhancement and nanodiamond surface properties.

2. Experimental

2.1. Equipment

All electrochemical experiments were carried out using a µAutolab PGSTAT potentiostat (Eco Chemie, Utrecht, Netherlands) running GPES (v4.9) or a CHI910B Scanning Electrochemical Microscope/bipotentiostat (CH Instruments, Inc. Austin, Texas, USA) running CHI (v6.28). Electrochemistry was performed using a three electrode setup. The working electrode was a boron-doped diamond disk (d = 3.0 mm), press fitted into a PEEK body (Windsor Scientific, Slough, United Kingdom). The counter electrode was fabricated in-house from platinum wire and sheet, cut into flags of approximately 4 cm^2. A stable reference potential was achieved by using an Ag/AgCl (sat. KCl) RE-5B reference half-cell (BASi, West Lafayette, America).

A Carbolite MTF 1200 horizontal tube furnace was used to pre-treat and clean all nanodiamond samples. The temperature control unit and associated electronics were designed and built in house. Mid-infrared spectra were recorded (100 scans) in attenuated total reflectance (ATR) mode using a Bruker Tensor 27 fourier transform infrared (FTIR) spectrophotometer (Bruker, Coventry, United Kingdom) fitted with a room temperature DLaTGS detector at 4 cm^{-1} resolution. The Platinum ATR accessory consisted of a diamond prism operating with one reflection. Background spectra were collected prior to each experiment (100 scans). Transmission electron micrograph (TEM) images were recorded using a Jeol JEM 2100 TEM with a 200 kV accelerating voltage using a LaB6 filament. All nanoparticles were deposited from the same solutions used for modifying electrode surfaces. Carbon coated copper TEM grids were used as the nano-particle support.

2.2. Chemicals and solutions

Nanodiamond (10 nm mean particle size, measured by TEM analysis, >97%), potassium chloride *(puriss* grade >99.5%), potassium dihydrogen phosphate (>98%), potassium phosphate dibasic (puriss, >99%), potassium hexacyanoferrate trihydrate (98.5-102.0%) and ferrocene methanol (97%) were all purchased from Sigma-Aldrich (Dorset, England). Other nanodiamond samples were gifted by a collaborator. All solutions were prepared using water from a Millipore Milli-Q Gradient A10 water filter (18.2 MΩ cm). Electrodes were cleaned by mechanical polishing with MasterPrep alumina polishing suspension, 0.05 µm (Buehler, Düsseldorf, Germany) and deionized water using 2-7/8" microcloth polishing pads (Buehler, Düsseldorf, Germany). Electrochemical measurements were carried out in either potassium chloride (0.1 M) with a recorded pH of 5.88, or a mixture of the phosphate buffer solutions potassium di-hydrogen phosphate (0.1 M) and potassium phosphate dibasic (0.1 M) mixed in different proportions to achieve the required pH.

All nanodiamond samples were treated in a furnace at 425 ºC for 4 h (including temperature ramp times, which were set at 10 ºC min^{-1}) in air. This was to remove any sp^2 graphitic carbon from the surface and maximise the number of oxygen terminating functional groups [17]. Nanodiamond suspensions were prepared by adding nanodiamond to purified water, centrifuging twice (13,200 rpm for 10 min) and briefly sonicating to ensure large aggregates were broken up. The mass per volume concentrations of the various nanodiamond solutions were: 5 nm ND 1.50 mg ml^{-1}; 10 nm ND 1.50 mg ml^{-1}; 100 nm ND 1.55 mg ml^{-1}; 250 nm ND 1.60 mg ml^{-1} and 1000 nm ND 1.7 mg ml^{-1}.

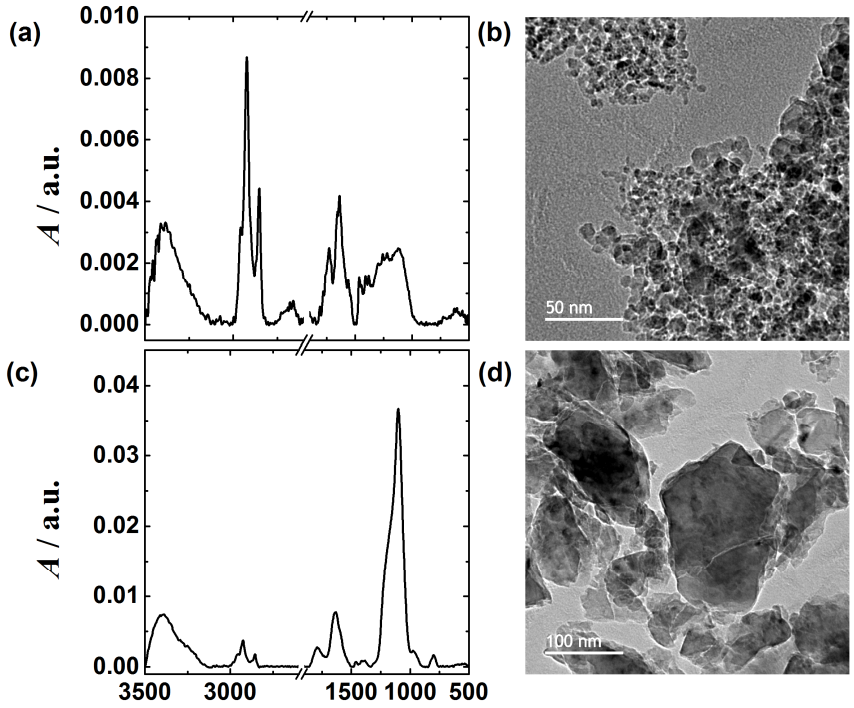

Fig. 2 – ATR-FTIR spectra and TEM micrograph of 5 nm, (a) and (b), and 100 nm, (c) and (d), nanodiamond drop-cast films

2.3. Preparation of nanodiamond-modified electrodes

Nanodiamond films were drop coated onto clean, dry electrodes by pipetting the various nanodiamond suspensions (2.5 µl) onto the electrode surface. The droplet was positioned and manoeuvred to ensure complete coverage of the electrode's surface. The nanodiamond coated electrode was left to air dry for 20 min and checked under an optical microscope to ensure even and complete coverage.

3. Results

3.1. Characterisation of nanodiamond materials using FTIR and TEM

Figure 2 shows representative FTIR spectra and TEM micrographs for two of the nanodiamond samples used in this study: 5 nm detonation nanodiamond and 100 nm microcrystalline nanodiamond (produced by mechanical grinding of synthetic diamond). Two different detonation nanodiamond materials were studied and examination with TEM (Figure 1 a, Figure 2 b) revealed the powder to be composed of discrete spherical and relatively monodisperse particles; one sample with mean particle diameter 5 nm and other with slightly larger particle diameter closer to 10 nm. In both samples the individual nanoparticles aggregate together to form larger agglomerates. The surface of all of the nanodiamond samples used is highly oxidised due to the pretreatment procedure of heating in air, described in 2.2 above. The

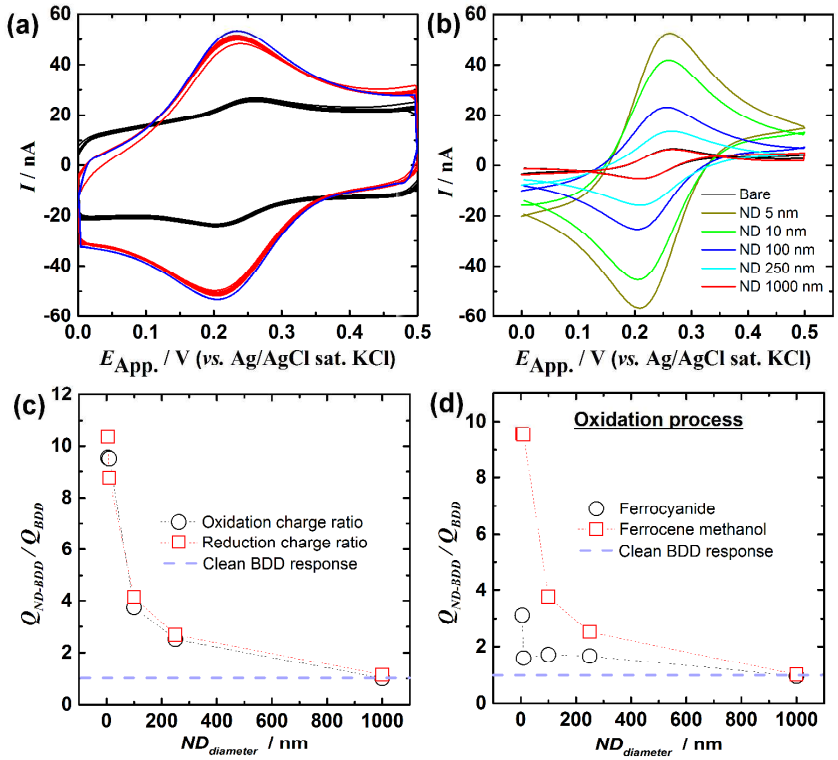

Fig. 3 – (a) Voltammograms of FcMeOH (1 µM) in KCl electrolyte solution (0.1 M, pH 5.88) on a BDD (black) and 100 nm nanodiamond-modified BDD working electrode (red first 10 scans, blue final 10 scans, 100 scans total). v = 10 mV s^{-1}. (b) Voltammograms (5th of 5 scans) of FcMeOH (1 µM) in KCl electrolyte solution (0.1 M, pH 5.88) on a BDD (black) and various different nanodiamond-modified BDD working electrodes (coloured lines, d = 5-1000 nm). v = 20 mV s^{-1}. (c) Charge ratio of the FcMeOH peak enhancement ($Q_{ND\text{-}BDD}$:Q_{BDD}) *vs*. nanodiamond size, calculated from data presented in (b). (d) Charge ratio of the FcMeOH/$Fe(CN)_6^{4-}$ peak enhancement ($Q_{ND\text{-}BDD}$:Q_{BDD}) *vs*. nanodiamond size calculated from data presented in (b) for FcMeOH and identical experiments carried out using $K_4Fe(CN)_6$. The blue dashed line highlights the charge ratio response for clean, un-modified BDD.

FTIR spectrum of the 5 nm nanodiamond is complex, with a great number of different functionalities contributing to the vibrational spectra. These functionalities have been characterised and discussed in detail previously [11,12] and include alcohols and carbonyl species: 3393 cm^{-1} (νOH), 2926 cm^{-1} (νCH_2), 2847 cm^{-1} (νCH), 1729 cm^{-1} (νC=O) and 1634 cm^{-1} ($\nu OH_{Abs.}$). The convoluted set of peaks between 1000-1500 cm^{-1} contains a mix of bending and stretching modes of various C-C, C-H and C-O containing functionalities). Of most interest to the present study are the presence of redox-active functionalities such as unsaturated ketone or 'quinone-like' moieties that can participate in redox cycling [11].

The 100, 250 and 1000 nm samples have pronounced crystal facets, consistent with nanodiamond produced through mechanical grinding of High Temperature High Pressure synthesis [18]. Analysis of the size distribution of the 100 nm nanodiamond sample gives a mean particle size of 98 nm with standard deviation 35 nm, modal average size being *ca*. 100 – 120 nm.

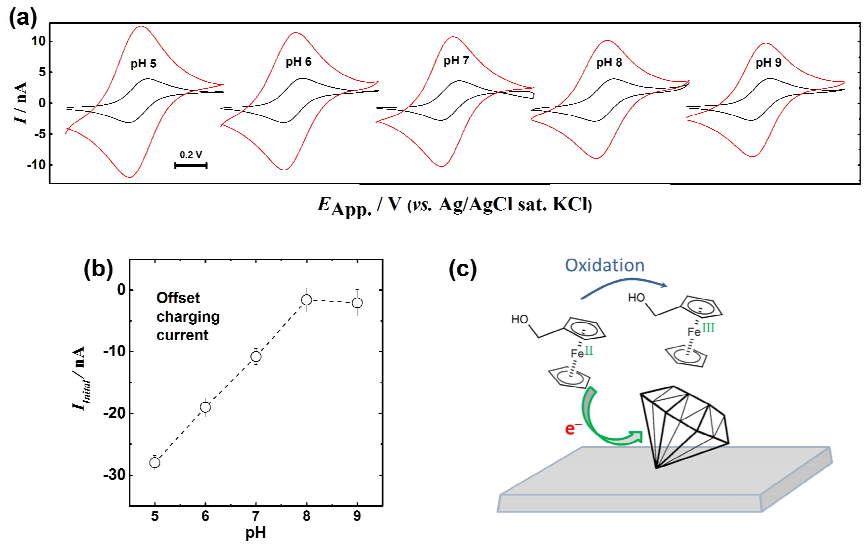

Fig. 4 – (a) Cyclic Voltammograms (1st scan) of FcMeOH (1μM) in aqueous solutions of K_2HPO_4:KH_2PO_4 (0.1 M) in various ratios to produce pH 5-9 electrolytes, at clean BDD electrodes (black) and nanodiamond modified BDD electrode (red) and were recorded at 5 mV s^{-1}. (b) Initial charging current's measured at different pH's 5-9 electrolyte (data collected from 1st scan of experiments displayed in (a)).(c) Illustration of FcMeOH oxidation performed by nanodiamond. The green arrow depicts the direction of electron transfer.

The crystalline nanodiamond samples all show a large absorption peak at *ca.* 1100 cm^{-1} in the IR spectra, attributable to nitrogen centres at defect sites within the bulk material [19]. The IR spectra of these larger nanodiamonds also show absorption bands attributed to surface functionalities at 3394 cm^{-1} (νOH), 2923 cm^{-1} (νCH_2), 2855 cm^{-1} (νCH), 1790 cm^{-1} (νC=O), 1631 cm^{-1} ($\nu OH_{Abs.}$) and 1103 cm^{-1} (νN-V$^-$) demonstrating the presence of similar surface functionalities to those on the detonation nanodiamond particles. Although the nanodiamond samples were produced by different synthetic methods making direct comparison difficult, the oxidative pre-treatment results in similar surface oxygen functionalities, allowing us to anticipate similar electrochemical properties.

3.2. Cyclic Voltammetry (CV) investigations of nanodiamond-modified electrodes

3.2.1 Effect of nanodiamond particle diameter on voltammetric response of FcMeOH

Figure 3 a shows the cyclic voltammograms (CV) of 1 μM FcMeOH at a clean boron doped diamond (BDD) electrode (black line) and a BDD electrode modified with 100 nm nanodiamond particles (red/blue lines). Both the oxidation and reduction currents at the nanodiamond modified electrode show similar enhancements of *ca.* four times that of the clean BDD surface. This current enhancement is stable to repeated cycling over multiple scans. Peak separation $\Delta E_p = |E_p^{ox} - E_p^{red}|$ is ~ 30 mV at the nanodiamond-modified electrode, in contrast to the theoretically predicted 59 mV for a diffusion-controlled one electron transfer. Figure 3 b shows CVs of FcMeOH at electrodes modified with nanodiamond of different diameter.

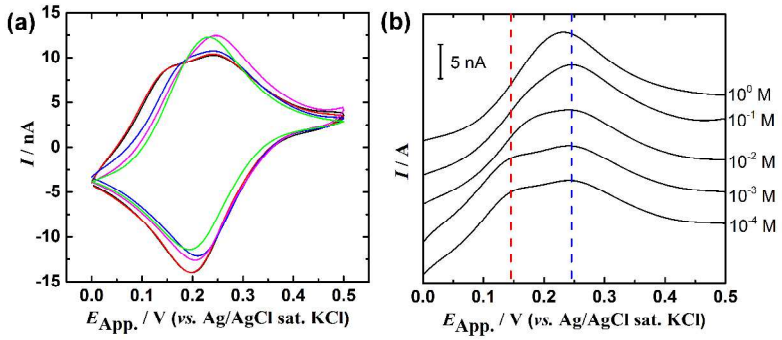

Fig. 5 – (a) Cyclic Voltammograms (5th scan) of FcMeOH (1μM) in aqueous solutions containing various concentrations of KCl (10^0-10^{-4} M, pH = 5.06-6.12 respectively) on a nanodiamond modified (100 nm) BDD working electrode at 5 mV s^{-1}. (b) Stacked plot of only the oxidation process. The blue dashed line identifies the standard FcMeOH diffusion controlled peak (as seen for at clean BDD), whereas the red dashed line highlights the emerging pre-peak.

The 1000 nm nanodiamond has negligible effect on the electrochemical response, the CV being essentially identical to that at clean BDD. Enhanced currents are observed at the other electrodes, with peak currents increasing in the order 250 nm < 100 nm < 10 nm < 5 nm. Oxidation and reduction peaks are enhanced equally in each case. The degree of current enhancement at the 10 nm and 5 nm nanodiamond-modified electrodes is quite dramatic. This has been quantified in Figure 3 c, where a 'charge enhancement ratio' has been calculated for each nanodiamond diameter. This is defined as the charged passed during oxidation or reduction at the nanodiamond-modified electrode divided by that passed at the clean BDD electrode under the same conditions i.e. $Q_{ND\text{-}BDD}/Q_{BDD}$. Charge passed during oxidation of FcMeOH or reduction of $FcMeOH^+$ is increased by a factor of ten when the electrode is modified with a layer of 5 nm or 10 nm nanodiamond. A four-fold enhancement is noted for the 100 nm particles, falling to two-fold for the 250 nm nanodiamond and no enhancement is seen for an electrode modified with 1000 nm particles.

In comparison to previous studies using the $Fe(CN)_6^{3-/4-}$ redox probe [9] the current enhancements for FcMeOH are considerable higher. This is shown in Figure 3 d, where the charge enhancement ratio for $Fe(CN)_6^{4-}$ oxidation is compared to that for FcMeOH oxidation at electrodes modified with different diameter nanodiamond. The data shows the same relationship between charge enhancement and nanodiamond diameter for both redox species, however, the magnitude of enhancement shows a strong dependence on the chemical nature of redox species, with FcMeOH currents being significantly more enhanced.

3.2.2. Effect of solution pH on CV response of FcMeOH at nanodiamond-modified electrodes

CVs for 1 μM FcMeOH at clean BDD and 100 nm nanodiamond-modified BDD in different pH solution of 5 – 9 are shown in Figure 4 a. At BDD the CV response of FcMeOH is independent of pH, producing voltammograms with ΔE_p *ca*. 60 mV, consistent with one-electron reversible, diffusion-controlled electrochemistry. The currents are enhanced at the 100 nm nanodiamond-modified electrodes over all pH

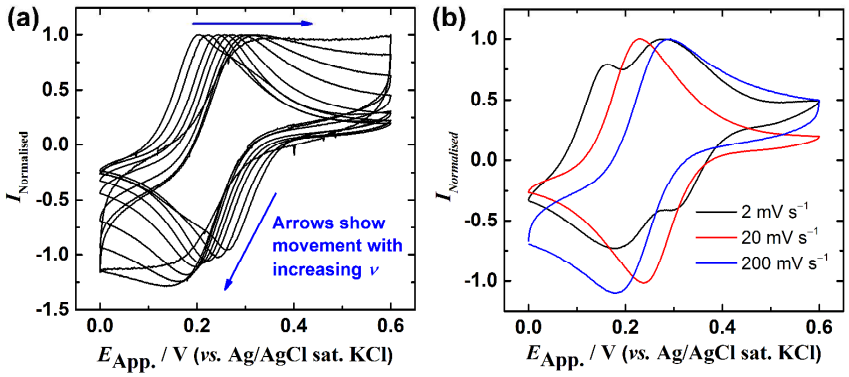

Fig 6 – (a) Normalised current (by max) voltammograms of FcMeOH (1 µM) for scan rates 1, 2, 5 10, 20, 50, 100, 200 and 500 mV s^{-1}. (b) Voltammograms of FcMeOH (10 µM) for scan rates 2, 20 and 200 mV s^{-1}. Experiments were performed with a 300 s pre-experiment equilibration time (no applied potential) in KCl electrolyte solution (0.1 M, pH 5.88) on a nanodiamond-modified (5 nm) BDD electrode.

values, but the enhancement is pH dependent with I_p increasing as the pH is lowered. As for Figure 3 a, ΔE_p for the nanodiamond-modified electrode is ~ 30 mV over the whole pH range. I_p *vs.* ν analysis suggests mixed diffusion controlled and adsorption behaviour.

Each of the CVs at the nanodiamond-modified electrodes exhibits a non-zero 'off-set' reduction current at 0 V. At this potential there should be no species in the solution available to be reduced (only FeMeOH is present and this can only be oxidised). We have reported this phenomenon previously for 5 nm nanodiamond-modified electrodes in solutions containing $Fe(CN)_6^{4-}$ [9]. It is attributed in the present case to reduction of $FcMeOH^+$ species within the diffusion layer at the electrode surface. $FcMeOH^+$ is proposed to be generated spontaneously by the oxidation of FcMeOH at the nanodiamond surface (Figure 4 c). This oxidation takes places through electron exchange between nanodiamond surface functional groups, which are reduced concomitantly with generation of $FcMeOH^+$. The magnitude of the off-set current is pH dependent as shown in Figure 4 b. At pH 5 significant initial reduction currents are observed, but these become negligible at pH 8 and above.

3.2.3. Effect of solution ionic strength on CV response of FcMeOH at nanodiamond-modified electrodes

The CVs for 1 µM FcMeOH at a 100 nm nanodiamond-modified BDD electrode in electrolytes of varying ionic strength is shown in Figure 5. The ionic strength was varied by altering the concentration of the KCl electrolyte across five orders of magnitude. As the ionic strength is decreased a pre-peak emerges from the oxidation wave, which shifts to more negative potentials with decreasing ionic strength (increasing the pre-peak to main-peak separation). The height of the main oxidation wave is decreased with decreasing ionic strength, while that of the reduction peak increases. In CV experiments the emergence of a pre-peak to an oxidation peak is usually taken as evidence of outer-sphere adsorption of the oxidation product at the electrode surface. In this case the oxidation product $FcMeOH^+$ is likely to experience a positive electrostatic interaction with the negatively charged

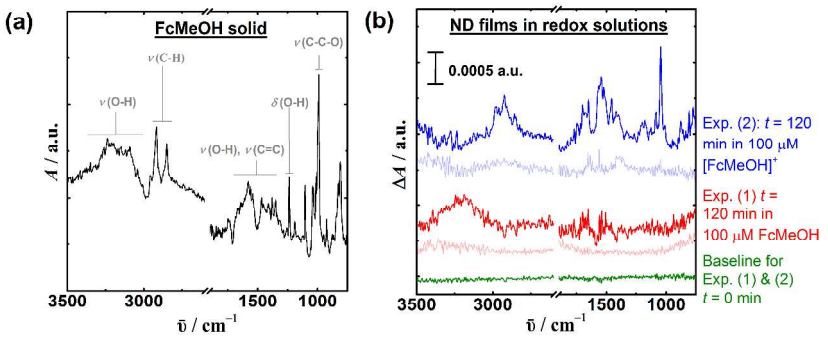

Fig. 7 – ATR-FTIR spectrum of FcMeOH (solid powder, black line) and (c) ATR-FTIR difference spectra (coloured lines) recorded for solutions of FcMeOH (red) and $FcMeOH^+$ (blue) on a clean ATR prism (transparent lines) and in the presence of a nanodiamond drop-cast film (solid lines). All aqueous solution contained KCl (0.1 M, pH 5.88).

nanodiamond surface [20,21]. Decreasing the ionic strength of the medium will increase the extent of adsorption as the length to which a surface or particle's electric field can be felt is inversely proportional to the concentration of electrolyte (as described by DLVO theory) [22,23]. This is consistent with the observations on Figure 5 b, where the adsorption pre-peak can be seen to become more prominent as ionic strength is decreased and hence more $FcMeOH^+$ adsorbs onto the nanodiamond surface.

3.2.4. Effect of CV scan rate on response of FcMeOH at nanodiamond-modified electrodes

The studies described in this section were carried out using 5 nm nanodiamond modified electrodes, as these showed the most extreme current enhancements. CVs were carried out in 1 μM and 10 μM FcMeOH over scan rates of 1 - 500 mV s^{-1} (Figure 6, where currents have been normalised for clarity). Below scan rates of 10 mV s^{-1} two oxidation waves are clearly observed; one wave is positioned at the same E_p at the diffusion-controlled oxidation peak at clean BDD and the other is a pre-peak to this main wave. A pre-peak to the reduction wave is also observed. As scan rate is increased the two waves merge to form one broad peak located midway between the pre-peak and main peak positions. At scan rates above *ca.* 100 mV s^{-1} only one peak is observed, at the position expected for a simple diffusion-controlled mechanism. However at very low concentrations of FcMeOH (1 μM) at the faster scan rates this peak becomes a steady state current response, indicating that oxidation is no longer taking place under diffusion-control.

3.3. In situ ATR IR spectroscopy of 5 nm nanodiamond in the presence of FcMeOH

The electrochemical data is strongly suggestive of adsorption of the oxidation product $FcMeOH^+$ in particular at the nanodiamond surface. In situ ATR-FTIR spectroscopy experiments were therefore performed to monitor changes in IR absorption at the nanodiamond/solution interface in solutions containing FcMeOH or $FcMeOH^+$. The experiments were performed by drop-casting a 5 nm nanodiamond film onto the ATR crystal. An enclosed liquid cell was clamped over the nanodiamond modified ATR crystal and gently filled with water to solvate the nanodiamond layer. After allowing time to equilibrate, a small volume of FcMeOH

or $FcMeOH^+$ solution was gently introduced to the cell and the FTIR spectrum between 3500-500 cm^{-1} recorded over 120 min. Figure 7 shows the IR difference spectra obtained after 120 min of nanodiamond film immersion in the FeMeOH or $FeMeOH^+$ solution, along with a spectrum of the solid FcMeOH for comparison.

In the absence of nanodiamond there is negligible change over 120 min in the IR spectra of the ATR crystal in FcMeOH solution. With the nanodiamond film the presence of FeMeOH produces increases in infrared absorption at *ca*. 3200 - 3300 cm^{-1} (νOH) and 1650 cm^{-1} (δOH) *i.e.* predominantly in regions associated with OH vibrational modes. There are a greater number of changes observed for the nanodiamond film exposed to $FcMeOH^+$ solution. These occur in regions associated with OH, C-H and C-O stretches and vibrations: 2925 cm^{-1} (νCH_2, asym.) 2845 cm^{-1} (νCH_2, asym.) 1648 cm^{-1} (δOH) 1576-1393 cm^{-1} ($\delta/\omega CH_2$) and 1044 (νC-C-O), showing many features in common with the solid FcMeOH spectrum [24].

4. Discussion

4.1. Mechanism of catalytic current enhancement

With the exception of 1000 nm nanodiamond, modification of the BDD electrode with an immobilised layer of nanodiamond results in enhanced CV currents for the reversible oxidation of FcMeOH. Catalytic current enhancements have previously been reported for the redox probes $Fe(CN)_6^{3-/4-}$, $IrCl_6^{2-/3-}$ and $Ru(NH_3)_6^{2+/3+}$ among others [1-3,6,9]; however currents achieved here for the neutral FcMeOH species are considerably higher than those observed for charged redox molecules. The current enhancement is partly attributed to a catalytic feedback mechanism, as shown in Figure 1 b. In this scheme FcMeOH undergoes oxidation at the BDD electrode to produce $FcMeOH^+$. FeMeOH is then regenerated rapidly by the reduction of $FcMeOH^+$ at the nanodiamond interface. On the CV return scan the opposite process is proposed to take place; FcMeOH generated at the electrode is immediately oxidised back to $FcMeOH^+$ after donating an electron to the nanodiamond surface. For this mechanism to be feasible requires the oxidation and reduction of nanodiamond surface functionalities at similar potentials to the standard potential of the solution redox probe. Electrode-immobilised 5 nm detonation nanodiamond has been shown to exhibit reversible redox peaks in this potential range, which shift potential with changing solution pH [9]. In addition *in situ* IR studies have provided evidence that 'quinone-like' surface moieties on the nanodiamond are involved in the redox cycling [11]. Although the 100 nm and 250 nm diamond particles used in this study are synthesised by different methods to the 5nm nanodiamond and possess different morphologies, the observed current enhancements suggest similar surface species on each that can contribute to a catalytic reaction mechanism. All of the samples were oxidised prior to use and among the oxygen functionalities present it is likely that 'quinone-like' and 'hydroquinone-like' species are present on each to support the catalytic cycle in Figure 1 b.

4.2. Relationship between particle size and current enhancement

In this study an inverse relationship between particle size and observed current enhancement was observed for both oxidation of FcMeOH and reduction of $FcMeOH^+$ in the presence of 5, 10, 100 and 250 nm diameter diamonds. The extent of enhancement observed, quantified as the 'charge enhancement ratio', depends on availability of nanodiamond surface functionalities to support the feedback

mechanism. The concentration of these functionalities will depend on nanodiamond particle size as well as the surface density of these groups. This latter factor will vary with oxidation pre-treatment, as well as the type of exposed crystal facets, edge sites and defect density. A log-log plot of charge enhancement ratio with nanodiamond diameter produces a straight line suggesting that a monomial power law relates these two properties. A straightforward relationship between the surface area to volume ratio of the particles and the charge enhancement ratio (σ) should result a $\sigma = 3r^{-1}$ fit to the data (where r is particle radius). However a more complex relationship is found. Fractal scaling could be one explanation for the unusual relationship obtained and it also should be noted that the 100 nm and 250 nm samples are not spherical, like the 5 and 10 nm samples. Most likely the density of redox active sites on the different diamond samples differs. The highly active detonation nanodiamond surface is very defective and has much in common with amorphous carbons; it exhibits an incredibly diverse and dense coverage of functionalities. In contrast the 100 nm and 250 nm samples are more 'diamond-like' in their character and thus surface defect density and degree of sp^2 bonding is much lower, resulting in fewer active sites. The 1000 nm diamond does not support the catalytic current enhancement (although neither does it block electrode activity). It is proposed that there are insufficient surface groups present on this material to produce a detectable catalytic current. The same mechanism is likely to take place at the surface of the 1000 nm diamond, however, the surface atom to bulk atom ratio is much smaller, so currents generated via this mechanism will be negligible in comparison to the diffusion controlled currents.

4.3. pH dependence of current enhancement

Current enhancement with 100 nm nanodiamond-modified electrodes was found to increase in the order pH 9 < pH 8 < pH 7 < pH 6 < pH 5. The redox response of FcMeOH at the BDD electrode is independent of pH, hence the ability of the nanodiamond to contribute to the catalytic cyclic must be the proton dependent step. 5 nm nanodiamond exhibits reversible redox peaks in voltammetry that shift by *ca.* 60 mV to more negative potentials with each increase in pH unit. This is typical of a coupled reaction of one proton per electron transferred and consistent with a quinone / hydroquinone redox transformation, which in aqueous solution is a $2H^+/2e^-$ reaction [9]. In the present study we propose that similar surface species are present on the 100 nm nanodiamond and that the redox potentials of these functionalities are similarly pH dependent. The pH 5 response suggests the potentials of the surface species are coincident with the potential of the FcMeOH / $FcMeOH^+$ couple at this pH. This match allows the most efficient electron transfer to take place between the nanodiamond and the solution species and hence the current enhancement is greater. As pH is decreased, the potential of the surface functionalities moves towards more negative potentials (according to Nernstian analysis of the proton dependence of the process), while that of the FcMeOH / $FcMeOH^+$ couple is unchanged. As the potentials of the solution and surface species are not so well matched, the driving force for the catalytic process is decreased and the current enhancement is not so pronounced. Hence smaller current enhancements are noted at pH 9.

4.4. pH dependence of the magnitude of off-set current

Further evidence for pH dependent electron transfer between nanodiamond surface groups and the FcMeOH species comes from inspection of the magnitude of the off-

set reduction current at 0 V in Figure 4. As described above we attribute this current to the reduction of $FcMeOH^+$ present in the diffusion layer. The $FcMeOH^+$ is proposed to be generated by the spontaneous oxidation of FcMeOH at the nanodiamond (ND) surface in the absence of applied potential:

$$FcMeOH + ND_{ox.} \rightarrow FcMeOH^+ + ND_{red.}$$

For such a process to be thermodynamically feasible, the nanodiamond surface functionalities must undergo reduction at a higher potential than the potential of the $FcMeOH/FcMeOH^+$ couple. The magnitude of the reduction current for the $FcMeOH^+$ species suggests this is the case at pH < 8 with the largest driving force for the process occurring at the lower pH values. At pH 8 and above the reduction currents are very small, indicating that electron transfer between the FcMeOH and the nanodiamond is negligible. This is consistent with the proton dependence of the potential of the surface functionalities. As pH increases the potential shifts to more negative values and by pH 8 is proposed to be found negative of that of the $FcMeOH/FcMeOH^+$ couple, hence spontaneous electron transfer does not take place.

4.5. Ionic strength dependence of voltammetric response

At low ionic strengths a pre-peak to both the main oxidation and reduction waves becomes evident. This, along with the observed increased width of the voltammetric peaks in the presence of nanodiamond as well as the decreased peak to peak separation (*ca*. 30 mV) is diagnostic of adsorption of both FcMeOH and $FeMeOH^+$ at electrode surface. As no evidence for adsorption is observed at the clean BDD electrode it is assumed that there is a strong affinity of the FeMeOH and $FcMeOH^+$ species for the nanodiamond surface. The positively charged $FcMeOH^+$ can clearly interact via electrostatic interactions with the negatively charged surface oxygen functionalities. Some current enhancement for the $Ru(NH_3)_6^{3+}$ species at 5 nm nanodiamond modified electrodes has previously been attributed to such an interaction. The strong adsorption of the neutral FcMeOH is more surprising as the nanodiamond surface is considered quite hydrophilic and less likely to interact with a largely hydrophobic molecule. However the adsorption of hydrophobic species to oxidised nanodiamond has previously been reported and in fact exploited for the delivery of water-insoluble drugs [25]. The sp^2 bonding present at the nanodiamond surface provides ample opportunity for hydrophobic and π-π stacking interactions with the aromatic pentacyclo- moieties of the FcMeOH molecule.

4.6. Contribution of adsorption processes to enhanced current response

The currents for FcMeOH oxidation at the nanodiamond-modified electrodes are much greater than observed previously for the $Fe(CN)_6^{4-}$ species. As the potential of the two species is similar, the same redox interactions with the nanodiamond surface groups are proposed. The difference in current enhancement is attributed to the extent to which the redox molecule can approach closely to the surface of the nanodiamond and the resulting efficiency of electron tunnelling between the two. The very negatively charged $Fe(CN)_6^{4-}$ is unlikely to be able to approach closely to the surface due to electrostatic repulsion, hence in the absence of any other factors it is not surprising that FcMeOH shows a higher current response that $Fe(CN)_6^{4-}$. However, the adsorption behaviour of FcMeOH and $FeMeOH^+$ is clearly a contributor to the very significant and unexpectedly large current enhancements we observe.

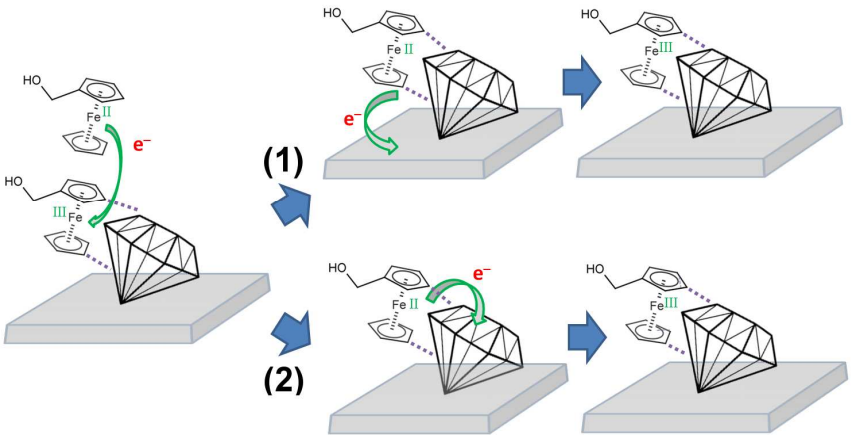

Fig.8 – Illustration of nanodiamond surface adsorbed $FcMeOH^+$ and its associated redox reaction. Re-oxidation of the FcMeOH product can then occur by either (1) the underlying electrode (when at sufficient potential) or (2) reaction with nanodiamond surface functionalities. The green arrows depict the direction of electron transfer.

As stated above, FcMeOH undergoes spontaneous oxidation at the nanodiamond surface to generate $FcMeOH^+$. This positively charged species will interact very strongly with the surface and become adsorbed. The strong interaction is illustrated by the affinity of the $FeMeOH^+$ for the nanodiamond surface, as found in the IR studies in Figure 7. The contribution of Gibbs energy of adsorption can shift the redox potentials of an adsorbed species relative to the solution species and results in the observation of pre-peaks in the CV [26,27]. Here we propose that the surface adsorbed $FcMeOH^+$ also participates in the catalytic feedback mechanism, as shown in Figure 8. Solution FcMeOH undergoes electron exchange with adsorbed $FcMeOH^+$ to generate solution $FcMeOH^+$ and adsorbed FcMeOH. The adsorbed FcMeOH can be re-oxidised to adsorbed $FcMeOH^+$ by the underlying BDD electrode, or by a redox process with nanodiamond surface groups. Thus in addition to the catalytic currents generated by the mechanism shown in Figure 1 b, the adsorbed species also mediate a catalytic process. The accumulative influence of both processes explains why currents are so significantly enhanced for this solution species compared to others previously studied.

4.7. Scan rate dependence of voltammetric response

The scan rate dependence of the response illustrates further the different processes contributing to the catalytic currents. At slow scan rates the pre-peak for the adsorption mediated process is very distinct from the main peak during the oxidation process. The two catalytic processes take place at distinct potentials; first via the adsorbed $FcMeOH^+$ species and then via the nanodiamond surface groups, indicating that adsorbed $FeMeOH^+$ is easier to reduce than the nanodiamond surface under these conditions. The factor determining the rate of the adsorption-mediated mechanism is the availability of adsorbed $FcMeOH^+$ to oxidise the solution FcMeOH. Assuming the rate of regeneration of adsorbed $FcMeOH^+$ by reduction at the BDD electrode or nanodiamond surface is fast enough, the limit to this reaction is simply how much $FcMeOH^+$ is adsorbed at the nanodiamond interface. The adsorption-mediated process is so distinctly observed at slower scan rates because

the flux of FcMeOH is smaller under these conditions and hence mass transport of reactant can keep up with the rate of regeneration of the available $FcMeOH^+$. At faster scan rates the higher flux of solution FcMeOH leads to diffusion-controlled currents overwhelming the adsorption response and pre-peak merges with the main diffusion-controlled peak. At higher scan rate and low concentration a steady-state current begins to emerge (Figure 6 a). In this regime we assume that catalysis take place largely by the nanodiamond-mediated mechanism shown in Figure 1 b. The steady state current shows that the rate of $FcMeOH^+$ generation at the BDD electrode is exactly matched by the rate of $FeMeOH^+$ reduction by the nanodiamond surface functionalities. At slow scan rates a peak response is obtained for this process, as a thick diffusion layer containing $FcMeOH^+$ builds up and there are insufficient nanodiamond surface functionalities to maintain the catalytic cycle. At faster scan rates the diffusion layer is much thinner, so there is less $FcMeOH^+$ for the nanodiamond to reduce, hence rate of electron transfer from the nanodiamond can keep up with the rate of $FeMeOH^+$ generation, leading to a steady state current response.

5. Conclusions

Modification of a BDD electrode with an immobilised layer of nanodiamond was found to enhance currents for the reversible oxidation of FcMeOH. Current enhancement is inversely related to nanodiamond diameter, with enhancement increasing in the order 1000 nm < 250 nm < 100 nm < 10 nm < 5 nm. In comparison to previous studies using negatively charged redox probes we find that currents are much larger for the neutral species FcMeOH under the same experimental conditions. We attribute the current enhancement to two catalytic processes: i) electron transfer between the solution redox species and redox active groups on the nanodiamond surface; ii) electron transfer mediated by $FcMeOH^+$ adsorbed onto the nanodiamond surface. The first process is pH dependent as it believed that 'quinone-like' and 'hydroquinone-like' species on the nanodiamond surface mediate the redox process and thus it is coupled to proton transfer. The $FcMeOH/FcMeOH^+$ redox cycle is more efficiently catalysed than the $Fe(CN)_6^{4-/3-}$ transformation reported previously, as the neutral and positive redox species are attracted rather than repelled by the negatively charged nanodiamond surface. The adsorption mediated process is observed most readily at slow scan rates and is due to electron self-exchange between adsorbed $FcMeOH^+$ and FcMeOH in solution. $FcMeOH^+$ has a strong affinity for the nanodiamond surface, as confirmed by in situ ATR FTIR experiments.

This study provides insight into the interaction of solution species with diamond and carbon surfaces under different physicochemical conditions. It also reveals mechanistic details of catalytic processes associated with the surfaces of nanodiamond materials. Catalytic currents within electrochemistry are of interest as they can allow energy extensive reactions to proceed at lower overpotentials (or allow a greater rate of reaction at the same overpotential). Such catalysts have applications in important sectors such as synthesis, energy conversion and molecular detection. Due to the particular mechanism of the nanodiamond electrocatalysis, nanodiamonds could find use within sensing devices, for example allowing detection of analytes at very low concentrations.

[a] *Department of Chemistry, University College London, Christopher Ingold Building, London, WC1H 0AJ, UK, Tel: +44 (0)20 7679 4623, e-mail: t.varley@ucl.ac.uk.*

1 For a review see: Holt, K. B.* (2014). Electrochemistry of Nanodiamond Particles. In *Nanodiamond*. Royal Society of Chemistry, Ed. Oliver A. Williams.
2 K.B. Holt, C. Ziegler, D.J. Caruana, J. Zang, E.J. Millán-Barrios, J. Hu and J.S. Foord, *Phys. Chem. Chem. Phys*., 2008, **10**, 303.
3 K.B. Holt, Phys. Chem. Chem. Phys., 2010, **9**, 2048.
4 W. Hongthani and D. J. Fermin, Diam. Relat. Mater., 2010, 19, 680.
5 J. B. Zang, Y. H. Wang, L. Y. Bian, J. H. Zhang, F. W. Meng, Y. L. Zhao, S. B. Ren and X. H. Qu, Electrochim. Acta, 2012, 72, 68.
6 J. B. Zang, Y. H. Wang, S. Z. Zhao, L. Y. Bian and J. Lu, *Diamond Relat. Mater*., 2007 **16**, 16.
7 L. H. Chen, J. B. Zang, Y. H. Wang and L. Y. Bian, *Electrochim. Acta*, 2008, **53**, 3442.
8 I. A. Novoselova, E. N. Fedoryshena, E. V. Panov, A. A. Bochechka and L. A. Romanko, *Phys. Solid State*, 2004, **46**, 748.
9 K.B. Holt, D.J. Caruana and E.J. Millán-Barrios, *J. Am. Chem. Soc.*, 2009, **131**, 11272.
10 V.N. Mochalin, O. Shenderova, D. Ho and Y. Gogotsi, *Nature Nanotech.*, 2012, **7**, 11.
11 J.-S. Tu, E. Perevedentseva, P.-H. Chung and C.-L. Cheng, *J. Chem. Phys*., 2006, **125**, 174713.
12 J. Scholz, A. J. McQuillan and K. B. Holt, *Chem. Commun.*, 2011,**47**, 12140.
13 O. Shenderova, A. M. Panich, S. Moseenkov, S. C. Hens, V. Kuznetsov and H.-M. Vieth, *J. Phys. Chem. C.*, 2001, **115**, 19005.
14 A. Dementjev, K. Maslakov, I. Kulakova, V. Korolkov and V. Dolmatov, *Diam. Relat. Mater.*, 2006, **15**, 1813.
15 W. Zhao, J.-J. Xu, Q.-Q. Qiu and H.-Y. Chen, *Biosens. Bioelectron.*, 2006, **22**, 649.
16 J.-T. Zhu, C.-G. Shi, J.-J. Xu and H.-Y. Chen, *Bioelectrochemistry*, 2007, **71**, 243.
17 S. Osswald, G. Yushin, V. Mochalin, S.O. Kucheyev and Y. Gogotsi, *J. Am. Chem. Soc.*, 2006, **128**, 11635.
18 A. Krueger, *Chem.-Eur. J.*, 2008, **14**, 1382.
19 I. Kiflawi, A.E. Mayer, P.M. Spear, J.A. Van Wyk and G.S. Woods, *Phil. Mag. B*, 1994, **69** 1141.
20 O. A. Williams, J. Hees, C. Dieker, W. Jäger, L. Kirste an C. E. Nebel, *ACS Nano*, 2010, **4**, 4824
21 M. Ozawa, M. Inaguma, M. Takahashi, F. Kataoka, A. Kruger and E. Osawa, Adv. Mater., 2007, **19**, 1201.
22 J.P Hsu and Y.C. Kuo, J. Colloid Interface Sci., 1997, **185**, 530.
23 P. Debye and E. Hückel, *Physikal. Z*., 1923, **24**, 185
24 G. Socrates, *Infrared characteristicgroup frequencies – Tables and charts*. 2nd Ed., 1994, Wiley and Sons.
25 M. Chen, E.D. Pierstorff, R. Lam, S-Y. Li, H. Huang, E. Osawa and D. Ho, *ACS Nano*, 2009, 3, 2016.
26 R.H Wopshall and I. Shain, *Anal. Chem*., 1967, **39**, 1514.
27 R.H Wopshall and I. Shain, *Anal. Chem*., 1967, **39**, 1535.

Acknowledgements

The authors would like to thank the EPSRC for funding this research (Grant No. EP/J010006/1). We also wish to extend our gratitude to Christoph Salzmann and Martin Rosillo-Lopez for use of their furnace and Steve Firth for assistance with TEM analysis,